J Mater Sci: Mater Electron (2022) 33:17923–17938

Synthesis and characterization of highly conductive poly(indole-4-aminoquinaldine) copolymer

Tuğçe Aşkın[1], Rukan Suna Karatekin[1,*], and Meltem Düdükcü[1]

[1] *Department of Chemistry, Faculty of Science and Letters, Mersin University, 33342 Mersin, Turkey*

Received: 23 March 2022
Accepted: 25 June 2022
Published online: 9 July 2022

ABSTRACT

Conductive polymers with good conductivity and large surface area are used as N-precursor materials for N-doped carbon-based catalysts and increase the catalytic activity of the electrode. Therefore, synthesis of the novel highly conductive polymer is an essential issue. This study reports that the synthesis of a novel copolymer is called poly(indole-4-aminoquinaldine) successfully achieved both chemically and electrochemically. The effect of scan rate, scan number, monomer concentration, and solvent on the polymerization process was investigated, and hereby the optimum synthesis conditions for the copolymer were determined. Under optimum conditions, the polyindole was also synthesized electrochemically and properties of polyindole compared to poly(indole-4-aminoquinaldine). The electrochemical characterization was investigated by cyclic voltammetry (CV) and electrochemical impedance spectroscopy (EIS). The electrical conductivity of the poly(indole-4-aminoquinaldine) and polyindole was measured using a four-point probe technique as 6 S/cm and 1×10^{-2} S/cm, respectively. Additionally, bandgap of copolymer and polyindole was found to be 3.10 and 3.18 eV, respectively. The structural, thermal, and morphological analysis of poly(indole-4-aminoquinaldine) and polyindole were carried out with UV–Vis Spectroscopy, Fourier-transform infrared spectroscopy (FT-IR), thermal gravimetric analysis (TGA), X-ray diffraction (XRD), elemental mapping, scan electron microscopy (SEM), and energy-dispersive X-ray analyzer (EDX) techniques. The novel copolymer synthesized in this study has high thermal stability and high electrochemical activity as well as high conductivity.

1 Introduction

In recent years, modified electrodes, which have gained popularity in many research areas, have been used to improve the performance of electrocatalysts. Depending on the dopant molecules used, the modified electrodes acquire unique properties, such as electrical conductivity, chemical stability, and reactivity, compared with pure electrodes [1].

Currently, graphene has been commonly used due to its high surface area, high thermal conductivity,

Address correspondence to E-mail: rukansuna@mersin.edu.tr

https://doi.org/10.1007/s10854-022-08655-2

and fast charged carrier mobility [2]. To increase the catalytic activity and adsorption capability of graphene, it is doped with heteroatoms such as N, S, P, and B [3]. Among dopant agents, nitrogen is very popular due to its electron pair that is shared with the π conjugation system of graphene [1, 4]. Therefore, in recent studies, the usage of N-doped electrodes has become widespread in the field of energy such as CO_2 reduction [5, 6], supercapacitors [7], lithium-ion batteries [8, 9], hydrogen energy [10], and fuel cells [11]. N-doped electrodes have been prepared by different methods, such as chemical vapor deposition in NO_2 or NH_3 atmosphere, hydrothermal carbonization, and decomposition of N-containing metal–organic precursors such as urea, melamine, and conductive polymers [12–17] Conductive polymers have been widely used for the preparation of these electrodes due to their high nitrogen content, easy synthesis, and control of morphology. Additionally, they have unique pore structures and specific surface areas by direct carbonization in an inert atmosphere [18].

Polyaniline and polypyrrole have been used extensively as a precursor material for obtaining N-doped electrodes [19–22] because their conjugated chains can provide the necessary electron transfer. In addition, unlike other N precursors, polymeric-N located in polymer conjugated chains, thus support the stability of the catalytic activity of the catalyst [23]. Moreover, nitrogen group gives carbon materials an acid-based character and enhances the capacitance. Due to all these advantages of N-containing polymers, they are widely used as a catalyst in the electrochemical reactions, especially in the field of supercapacitors [24]. Polyindole is another conductive polymer that contains N-group. It has many potential applications, such as supercapacitors [24, 25], diodes [26, 27], biomedicine [28–30], sensors [31, 32], and corrosion protection [33–35] due to its low toxicity, slow degradation rates, and excellent redox activity. However, among the conductive polymers, polyindole has a lower conductivity and it limits its usage in applications [36, 37].

This limitation has been overcome by doping polymer with a monomer, an ion, and an anionic or cationic surfactant. For example, Wang et al. improved the conductivity of polyaniline by adding camphorsulfonic acid (CSA) with poly(amid-imid) [38].The same group in a different study developed a ternary conductive polymer composite for improving polyaniline conductivity [39]. Qi et al., also synthesized highly conductive polypyrrole by using a freezing interfacial polymerization [40]. Sirivat et al. synthesized highly conductive polyindole (14 S/cm) with sodium dodecyl sulfate (SDS) and ClO_4^- anions. They emphasized that it is the best conductivity value for polyindole in the literature [41].

As mentioned above, when using conductive polymer as an N precursor, modified electrodes have gained unique properties for different research areas. However, to synthesize polymers with highly conductive values, more stages or expensive processes are needed. So, it is necessary to develop a highly conductive novel polymer or copolymer that can be synthesized with one inexpensive step. In this study, we aimed to present a polymer with high N content, easily prepared, high conductivity, and low cost, which acts as a precursor material for the preparation of N-doped electrodes. For this purpose, a surfactant-free copolymer that included a second monomer that would increase both the conductivity and the N content of the polyindole was synthesized by an inexpensive process. Improving the N content in the electrode is necessary to increase the electroactivity of the catalyst. Therefore, 4-aminoquinaldine (4-aq), which consists of 6-membered two aromatic rings and is a heterocyclic compound with the $–CH_3$ and $–NH_2$ functional groups, was preferred [42, 43]. 4-aq has been used in the production of antibacterial and antifungal drugs [44], for corrosion inhibition [45] and for analytical detection of metal ions [46]. Additionally, limited studies show that it can be synthesized as an electroactive polymer. In the mentioned studies, poly(4-aminoquinaldine) was synthesized electrochemically on the Pt and glassy carbon electrodes, respectively [47, 48].

Our aim was to improve the properties of polyindole in a simple way, adding a second monomer to obtain a novel copolymer. For this purpose, optimum synthesis conditions were investigated to use the obtained copolymer as N precursor. For this the effect of scan rate, cycle number, monomer concentration, and ratio of solvent on the electrocatalytic activity of the novel copolymer was investigated and optimum conditions were determined. Under the same conditions, polyindole was synthesized electrochemically on indium tin oxide-coated glass (ITO). Additionally, copolymer and polyindole were successfully synthesized chemically using the same solution media and $FeCl_3$ as an oxidant.

The structural properties of the copolymer and polyindole were characterized with SEM–EDX, XRD, UV–vis, FTIR, and TGA. Also, the electrocatalytic activity of polyindole and copolymer was investigated by CV, EIS, and also ICP-MS indirectly.

2 Methods and materials

2.1 Chemicals

Indole (C_8H_7N, Merck, Germany), 4-aminoquinaldine ($C_{10}H_{10}N_2$, Sigma-Aldrich, China), Acetonitrile (C_2H_3N, Merck, Germany), Perchloric acid ($HClO_4$, Merck, Germany), Sulfuric acid (H_2SO_4, Merck, Germany), methanol (CH_3OH, Merck, Germany), ethanol (C_2H_6O) Merck, Germany), ethylene glycol ($C_2H_6O_2$, Merck, Germany), hexane (C_6H_{14}, Merck, Germany), tetrahydrofuran (C_4H_8O, Merck, Germany), dichloromethane (CH_2Cl_2, Merck, Germany), $CuCl_2$ (Merck, Germany), KCl (Merck, Germany), $FeCl_3$ (Merck, Germany) were used. All aqueous solutions were prepared with ultrapure water (Millipore, 18.2 MΩ cm).

2.2 Method

2.2.1 Chemical synthesis of polyindole and copolymer

For the chemical synthesis of polyindole, 0.5 M $FeCl_3$ was added slowly in 1:4 acetonitrile (ACN)-1 M $HClO_4$ solution containing 0.1 M indole. After mixing for 4 h, it was filtered and rinsed with water. The synthesized polymer was dried at 60 °C for 24 h.

For the chemical synthesis of the copolymer, 0.1 M indole and 0.1 M 4-aq were dissolved in acetonitrile and 1 M $HClO_4$ mixed in a ratio of 1:4, and then 0.5 M $FeCl_3$ was added dropwise to the mixture. The next steps carried out the same procedure above.

2.2.2 Electrodeposition of polyindole

The electrochemical measurements were conducted using CHI-660C electrochemical workstation. The three-electrode system consisting of an ITO (1 × 1.5 cm^2) as a working electrode, a Pt sheet (1 × 1.5 cm^2) as an auxiliary electrode, and an Ag/AgCl as a reference electrode was used.

The polyindole film was grown from a solution prepared in a ratio of 1:4 acetonitrile and 1 M $HClO_4$ containing 16 mM indole. Polymerization was performed at various scan rates with various cycle numbers under potentiodynamic conditions.

2.2.3 Electrodeposition of poly(indole-4-aminoquinaldine)

poly(indole-4-aminoquinaldine) was grown from a solution that was prepared with a ratio of 1:4 acetonitrile and 1 M $HClO_4$ containing 16 mM indole and 16 mM 4-aminoquinaldine. To understand the effect of the concentration of 4-aq on copolymer, the polyindole concentration value was fixed at 16 mM, and 4-aq concentrations were selected as 8 mM and 32 mM, respectively. That is, the monomer concentration ratio was chosen to be 0.5:1, 1:1, and 2:1.

2.2.4 Electrochemical characterization of polyindole and copolymer

The electrochemical activity of each electrode was compared, which was obtained under different synthesis conditions such as scan rate, scan number, and monomer concentration using the CV method.

For this purpose, the polymer electrodes were immersed in 0.1 M $CuCl_2$ solution for 45 min and then *I–V* curves were recorded in 0.1 M KCl from − 0.2 to 0.8 V (Ag/AgCl) at a scan rate of 20 mV/s.

The EIS measurement was performed within the frequency range of 10^{-2} to 10^5 Hz in 0.5 M H_2SO_4. The amplitude of the applied sine wave potential was 5 mV with the direct current potential set at 0.6 V (Ag/AgCl). The impedance data were calculated using Zview2.

2.2.5 Characterization of polyindole and poly(indole-4-aq)

2.2.5.1 SEM analysis The surface morphology of polymer films that was synthesized electrochemically was investigated by field emission scanning electron microscope (FE-SEM). The SEM images were taken using a Zeiss (Supra 55) SEM instrument. The chemical composition and mapping of the electrode surfaces were determined by an energy-dispersive X-ray spectrometer (EDS).

2.2.5.2 XRD analysis The chemical structures of electrodes were examined by a wide-angle X-ray spectrometer (XRD, Empyrean, PANanalytical)

operated in the 2θ scan from 10 to 70° and Cu-Kα irradiation used as an X-ray source (40 kV/30 mA). The scan was made at a rate of 2.5° per minute.

2.2.5.3 FT-IR analysis FTIR spectra of indole, 4-aq, polyindole, and poly(indole-4aq) were recorded by a JASCO-6800 spectrometer. A measuring range of 450–4000 cm^{-1} was selected. Chemically polymerized polyindole and poly(indole-4aq) powder was used for this analysis.

2.2.5.4 TGA analysis TGA (Mettler Toledo) analysis of polyindole and poly(indole-4aq) was carried out from 25 to 800 °C with a heating rate of 15 °C min^{-1} under N_2 atmosphere. For this analysis, polyindole and poly(indole-4-aq) were synthesized chemically, and 50 mg of each sample was used to perform the TGA analysis.

2.2.5.5 UV–Vis analysis UV–Vis spectra of polyindole and poly(indole-4aq) were recorded in the 200–700 nm range, using Shimadzu 1700 spectrophotometer. To obtain solutions of polyindole and copolymer, initially, polyindole and copolymer were synthesized chemically and then prepared their solutions with acetonitrile. The concentration of solutions was calculated to be 2.5 × 10^{-2} ppm.

2.2.5.6 Four-point probe measurement Electrical conductivities of the polyindole and poly(indole-4-aq) that was synthesized chemically were measured using a four-point probe (ENTEK) technique.

2.2.5.7 ICP-MS analysis To investigate the amount of Cu^{+2} adsorbed on polyindole and poly(indole-4aq), ICP-MS (Agilent 7500ce) was used.

3 Results and discussion

3.1 Effect of solvent on polymerization

In the literature, acetonitrile has been widely used as a solvent for electrochemical and chemical polymerization of polyindole [33, 35, 49].

In the limited number of studies in the literature, acidic media were used for the polymerization of 4-aminoquinaldine [47, 48]. To compare the electrochemical activity of polyindole and copolymer, a solution media that could dissolve both monomers were chosen. Hence, an acetonitrile and 1 M perchloric acid mixture were prepared with a ratio of 1:4, 2:3, and 3:2.

Although each monomer could be dissolved in a different ratio of the solution, polymer film was grown only in the solution with the mixture ratio of 1:4. Hence, polymerization experiments were performed in acetonitrile and 1 M $HClO_4$ (ACN: $HClO_4$ = 4:1 by vol.) mixtures of electrolytes.

3.2 Structural characterization

3.2.1 SEM–EDX analysis

SEM images with various magnifications (10.00 KX, 50.00 KX, and 100.00 KX) of polyindole and 0.5:1, 1:1, 2:1 copolymers are shown in Fig. 1. As can be seen from the SEM images, all polymers have an oval-like structure containing small particles on the surface. The average size particles of polymer structures were determined by the size distribution graph (Fig. S1). It was observed that with the increasing of the 4-aq concentration the size of the oval-like particles decreased, while the small particles size on these structures gradually increased. From these figures, it can be deduced that polyindole film has a more compact surface and smaller particle size than copolymer. Additionally, among all surfaces, copolymer (1:1) has a more regular and porous surface. The elemental analysis of polyindole and poly(indole-4aq) was carried out by EDX (Fig. 2a and b). From the results, it can be concluded that C and N elements belong to the polymer, while In, Si, and O elements belong to the electrode. As seen from Fig. 2a and b, the N content of polyindole is 8.95 (w. %), while the N content of the copolymer is 10.00 (w. %).

3.2.2 UV–Vis analysis

Figure 3a displays the UV–Vis absorption spectra of polyindole and copolymer. Polyindole and copolymer have similar absorption bands at 280–400 nm. In this range, the π–π^* electronic transition in the benzenoid segments has been observed [50]. It is seen from UV–Vis spectra that copolymer spectra are slightly different from polyindole spectra. It was noticed that copolymer has a new absorption band at approximately 250 nm, and it was observed that the absorbance bands of polyindole are broader than copolymer bands (Fig. 3a). These two differences

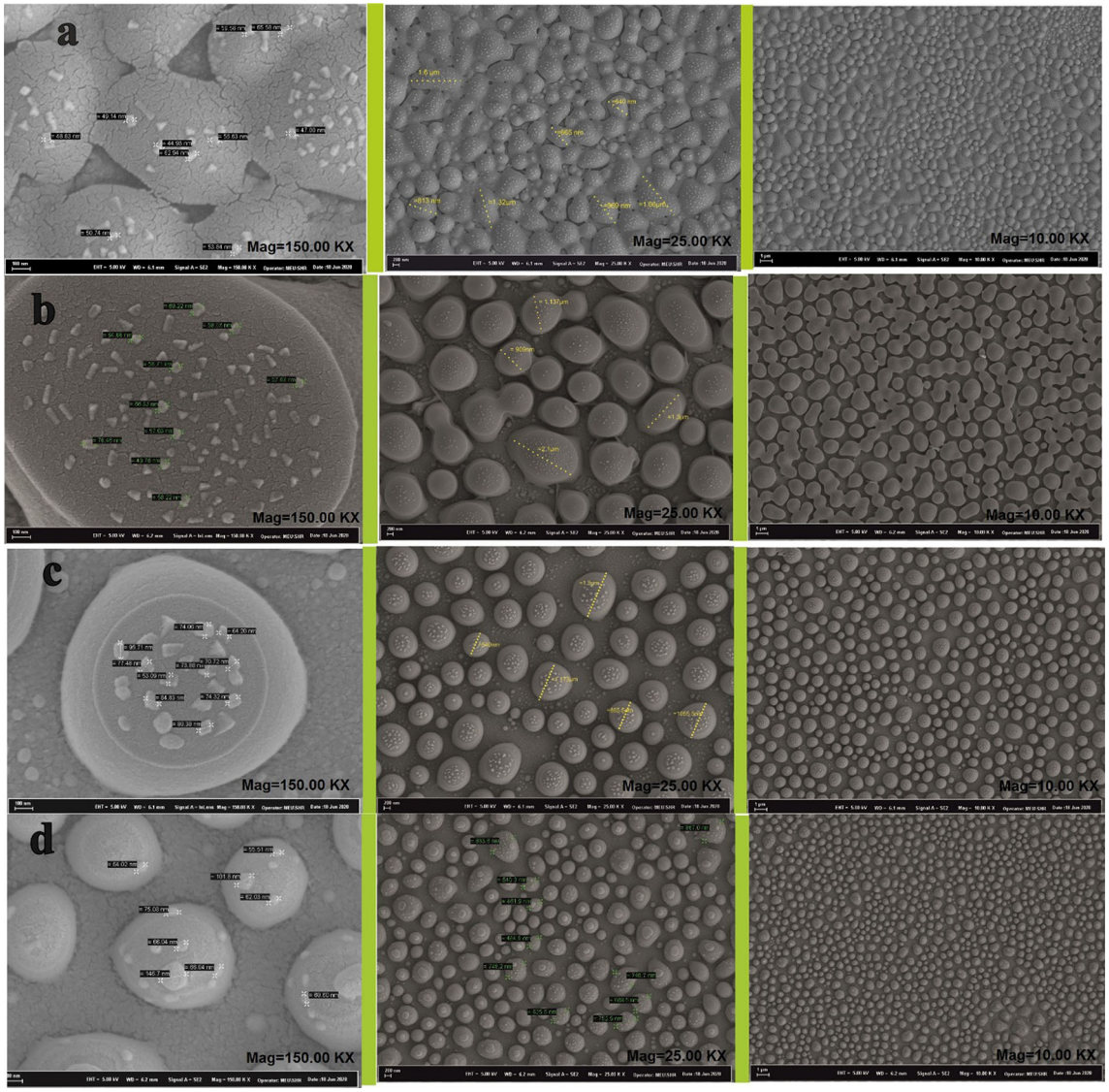

Fig. 1 Scanning electron micrographs of **a** PIN, **b** 0.5:1, **c** 1:1, **d** 1:2 copolymer

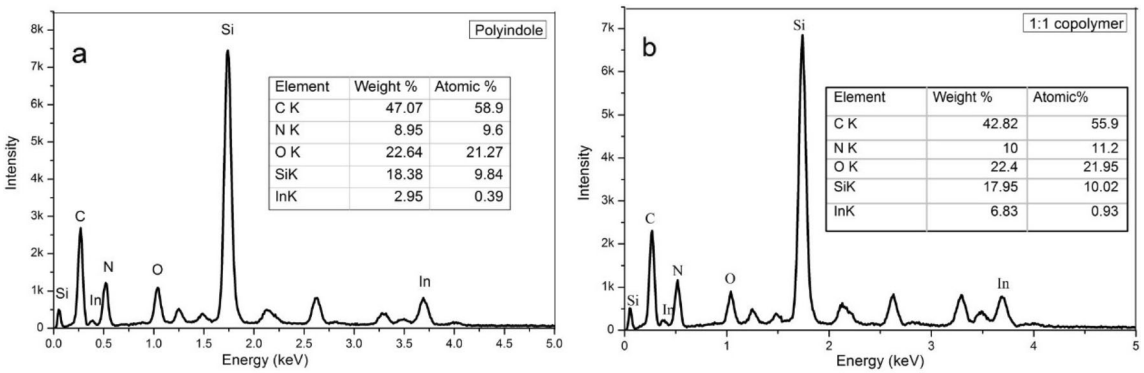

Fig. 2 EDX analysis of **a** polyindole with table including its elemental composition, **b** 1:1 copolymer with table including its elemental composition

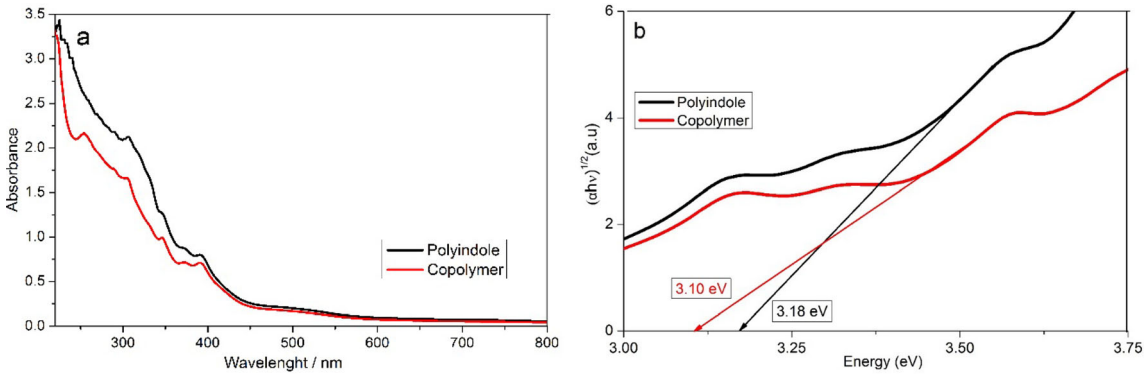

Fig. 3 **a** UV–Vis spectra of copolymer and polyindole. **b** Plot of $(\alpha hv)^{1/2}$ versus photon energy (eV) for polyindole and copolymer

support that the copolymer has different conjugation lengths when compared to polyindole [50]. A broader absorbance band was observed at 450–550 nm for both, which is ascribed to π-polaron transition.

In addition, from the UV–Vis spectra, the band gap of polyindole and copolymer were calculated using the Tauc's Eq. (1):

$$(\alpha hv) = A\left(hv - E_g\right)^n \quad (1)$$

where A is a constant parameter, α is the absorption coefficient, hv is the photon energy, and n indicates the type of optical transitions. The exponent n is 0.5 for direct allowed transitions, 1.5 for direct forbidden transitions, 2 for indirect allowed transitions, and 3 for indirect forbidden transitions. Thus, optical band gaps, E_g, can be calculated from the linear relation of $(\alpha hv)^{1/n}$ as a function of hv and can be determined by linear fit extrapolations to the x-axis of the plots (Fig. 3b). The value of n gives the best linear graph in the band edge region [51]. For each polymer, the value of n was selected as $n = 2$ which allows indirect transitions. According to the Tauc plots, indirect band gap values of copolymer and polyindole were determined to be 3.10 eV and 3.18 eV, respectively. The band gap is the minimum energy required to excite electrons participating in conduction. The decrease in the optical band gap is related to increase in the density of localized state in the polymer chain [52]. The fact that the band gap value of the copolymer and polyindole is different implies that the copolymer has a different structure and conductivity. According to the band gap values, copolymer has a higher conductivity compared with polyindole.

3.2.3 TGA analysis

Thermal stability of polyindole and poly(indole-4-aq) was investigated by thermo-gravimetric analysis. Figure 4 shows the TGA curves of the copolymer and polyindole. The results show that there are three major steps of weight loss for both. The initial weight-loss step occurred between 50 and 98 °C and was due to the evaporation of physically adsorbed water and solvent. The second weight-loss step occurred between 200 and 300 °C which might correspond to the removal of dopant anions.The last step occurred between 300 and 500 °C and could be due to thermal decomposition of polymer chains [50]. It was observed that for each step, the decomposition of copolymer is slower than for polyindole.

3.2.4 FT-IR analysis

FT-IR spectrum of indole, 4-aq, polyindole, and copolymer is shown in Fig. 5a. As seen from the spectrum of polyindole, a small peak observed at

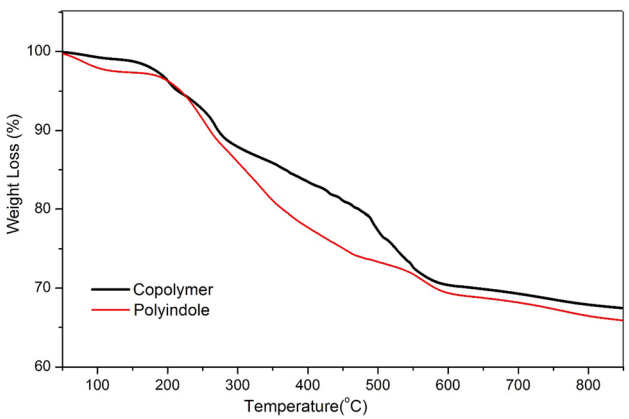

Fig. 4 TGA curves of the copolymer and polyindole

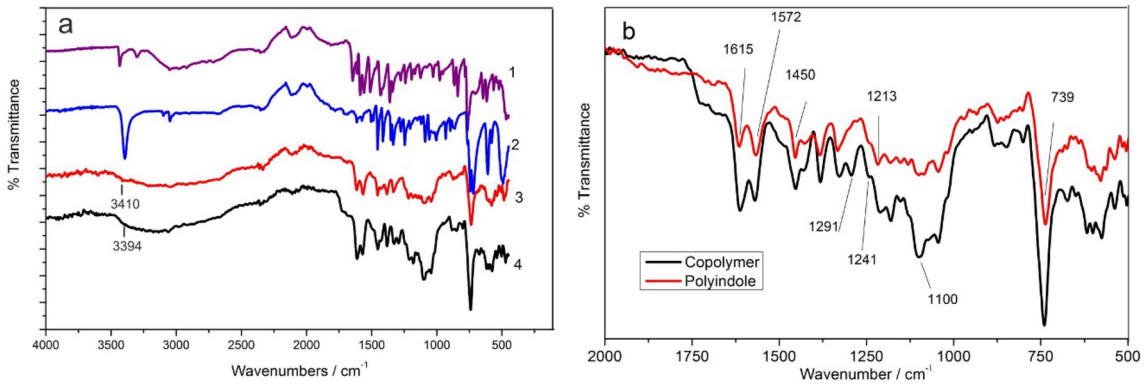

Fig. 5 FTIR spectra of **a** 4-aq (1), indole (2), polyindole (3), and copolymer (4) and **b** FTIR spectra of polyindole and copolymer in the range between 2000 and 500 cm^{-1}

3410 cm^{-1} is assigned to the N–H stretching vibration which confirmed the presence of polyindole [53]. For spectrum of copolymer, mentioned peak shifts to 3394 cm^{-1}. The peak at 1574 cm^{-1} shows that there are still N–H bonds on the polyindole backbone. This situation has proved that the N site was not the polymerization site and the polymerization coupling sites are at positions 2 and 3 [41, 54, 55]. The peak observed at 739 cm^{-1} indicates that the benzene ring is not involved in the polymerization process. Furthermore, the peaks observed at 1450 cm^{-1} and 1610 cm^{-1} are due to the stretching mode of the benzene ring of polyindole [54].

On the other hand, Fig. 5b shows that the spectra of polyindole are similar to copolymer's spectra. However, a marked increase in the intensity of the copolymer peaks has been observed relative to that of polyindole. This observation indicates that the copolymer has a more functional group compared to polyindole. Moreover, in the case of the copolymer, new bands appeared at 1291 cm^{-1} and 1241 cm^{-1}, which are due to the presence of C-CH_3 and C-N bonds in 4-aq [56]. It can be concluded from FTIR analyses that there is an interaction between indole and 4-aq. Additionally, the peak observed around 1100 cm^{-1} is thought to belong to the perchlorate anion preferred as a solvent [57]. All observed band position and assignments are listed in Table 1.

3.2.5 XRD analysis

X-ray diffraction patterns of polyindole and 0.5:1, 1:1, and 2:1 copolymers are shown in Fig. 6a. The broad peak in the region 2θ = 20–30° is related to the amorphous structure of the glass electrode. The peaks at 2θ = 30.29°, 35.21°, 50.69°, and 60.8° match Joint Committee on Powder Diffraction and Standards "JCPDS." card no: 01-089-4596 of the ITO and are related to the (222) (400) (440) (622) planes, respectively. The intensity of the peaks was decreased with the thickening of polymer film on ITO and increasing 4-aq concentration. In the region 2θ = 20–30°, the observed broad peak belongs to not only ITO but also amorphous polyindole and copolymer (Fig. 6b). However, the sharp peak observed at 2θ = 19° supported the partially crystalline nature of polyindole [50, 58]. The aforementioned peak that was observed at 2θ = 19° shifted to a lower angle (from 19 to 15°) accompanied by a weakened intensity which indicates that copolymer has a larger particle size [59] and has less crystallinity compared to polyindole [60]. Also, the XRD pattern of the copolymer (2:1) exhibits a new peak at 2θ = 25°, which may be due to the predominant concentration of 4-aq in the copolymer structure.

3.3 Testing of solubility polyindole and copolymer

The solubility of polyindole and copolymer was tested in different solvents. Methanol, ethanol, ethylene glycol, distilled water, hexane, tetrahydrofuran, acetonitrile, and dichloromethane were used for the solubility tests. The concentration used in the solubility test was 5 mg of each polymer in 1 ml of solvents at room temperature. All were tested to dissolve in a sonic bath for 5 min. Polyindole and copolymer were dissolved homogenously in the organic solvents except hexane. However, polyindole and copolymer were partially dissolved in water.

Table 1 Band position and assignments of polyindole and copolymer

Band position (cm^{-1})		Assignments
Copolymer	Polyindole	
3394	3410	N–H stretching vibration
1572	1574	Deformation N–H bonds
1450 cm^{-1} and 1615 cm^{-1}	1450 cm^{-1} and 1610 cm^{-1}	The stretching mode of the benzene ring
1291 cm^{-1}		C–N stretching
1241 cm^{-1}		$C–CH_3$ stretching
1100 cm^{-1}		perchlorate anion
739	741	–C–H deformation of the benzene ring

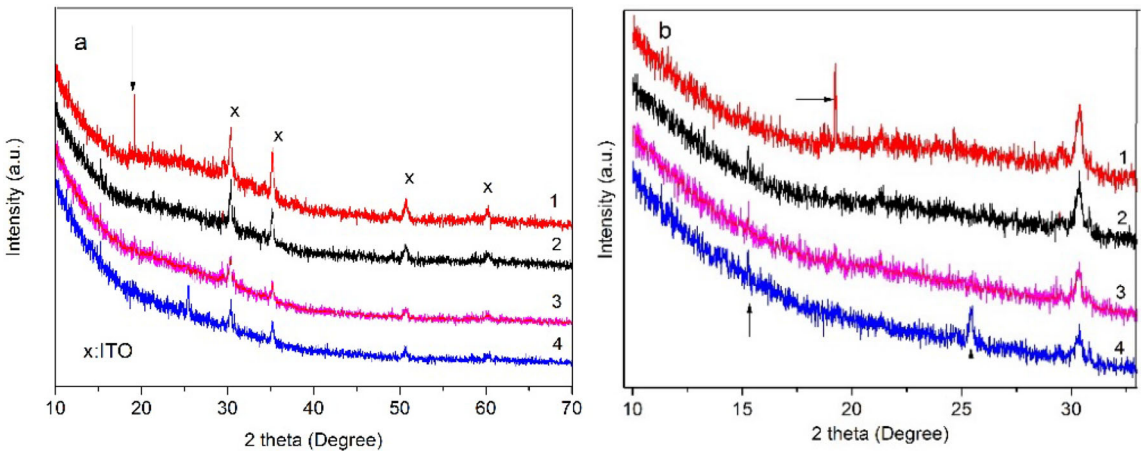

Fig. 6 XRD diffraction patterns for **a** polyindole (1), 0.5:1 copolymer (2), 1:1 copolymer (3) and 2:1 copolymer (4), in the region 2θ = 10–70°. **b** polyindole (1), 0.5:1 copolymer (2), 1:1 copolymer (3), and 2:1 copolymer (4) in the region 2θ = 10–30°

Therefore, it was concluded that both polyindole and copolymer have a substantially polar character.

3.4 Electrochemical experiments

3.4.1 *Synthesis of copolymer*

Figure 7 (inset figure) shows the cyclic voltammogram recorded between − 0.2 and 0.85 V on ITO in monomer-free acetonitrile-1 M $HClO_4$ solution (ACN: $HClO_4$ = 4:1 by vol.) at 80 mV/s. It is observed in Fig. 9 that the recorded current has microampere level under these conditions. The potentiodynamic polymerization was performed in the presence of 16 mM indole and 16 mM indole-4aq in the same conditions. The first scan of the voltammogram for polyindole and poly(indole-4aq) is shown in Fig. 7.

In the first anodic scan, no current was observed until the 0.53 V and 0.62 V for indole-4aq and indole, respectively. When the scan direction was switched, a nucleation loop was observed related to form conducting polymers for both voltammograms [60, 61]. In a cathodic scan, three reduction peaks were observed at around 0.45 V, 0.33 V, and 0.1 V for poly(indole-4aq) and 0.465, 0.31 V, and 0.085 V for polyindole. Furthermore, it was seen that the cathodic current peak intensities increased for copolymer. It is suggested that these cathodic currents belong to dimers and oligomers of indole and/or 4-aminoquinaldine [62].

The onset potential of the reaction is also concluded from the cyclic voltammogram. The onset oxidation peaks of polyindole and copolymer were observed at 0.62 V and 0.53 V, respectively. It is concluded that these peaks belong to monomer radical cation formations and the polymerization of indole occurs by a radical cation-neutral monomer or a radical cation- radical cation combination. In addition, the low onset potential of the copolymer indicates its easier growth than polyindole on ITO [62]. Also, the decreasing oxidation potential of the monomer indicates that the molecular weight of the polymer and hence the π-conjugated system in the

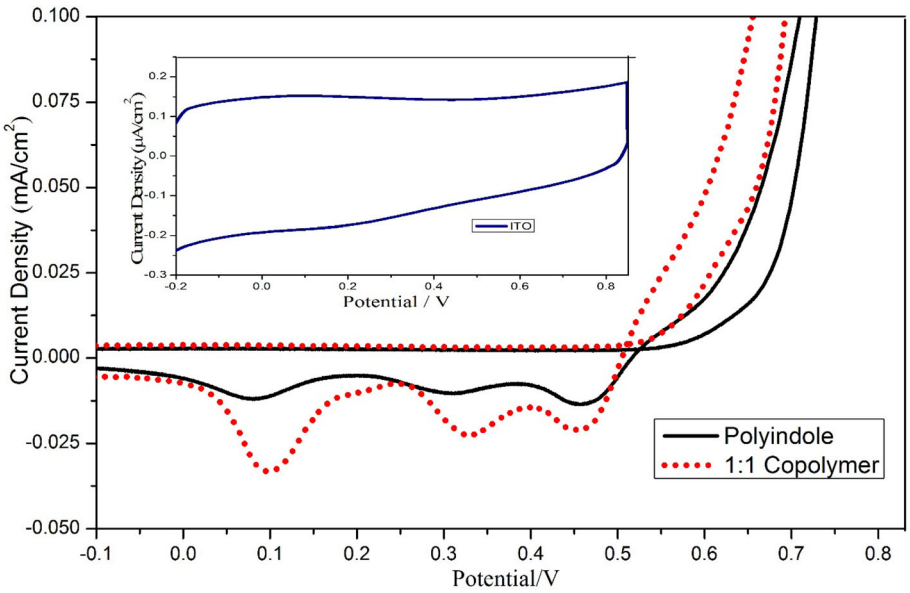

Fig. 7 Cyclic voltammogram of first cycling for growing of 16 mM indole (black line) and **b** 1:1 molar ratio of indole-4aq (dot line) on ITO electrode and bare ITO (inset figure) in acetonitrile and 1 M $HClO_4$ (ACN:$HClO_4$ = 4:1 by vol.) mixture electrolyte. Potential scan rate: 80 mVs^{-1}

polymer chain increases [63]. So, the conductivity of polymer increases with increasing π-conjugated system in the polymer chain. This result was supported by conductivity measurements. The conductivity of poly(indole-4aq) was found as 6 S/cm. This value is 600 times higher than the conductivity of polyindole that is synthesized under the same conditions.

Figure 8 shows the cyclic voltammograms recorded for the first four cycles of polyindole and poly(indole-4aminoquinaldine). It can be seen clearly from Fig. 8 that the peak currents increased with the increasing cycle numbers, especially for copolymer. The higher current response indicates higher conductive film deposition on ITO compared to polyindole. So that, according to the result of the Tauc plot and the conductivity measurements, copolymer has a higher conductivity value than that of polyindole.

Figure 9a presents the cyclic voltammograms of polymerization of indole and indole-4aq. In voltammograms, the increase of the intensities of both anodic and cathodic current peaks with the increase of the cycle number indicates the growth of the polymer film on ITO [60]. The growth of the copolymer with higher current density compared to polyindole indicates an increase in polymer mass on ITO according

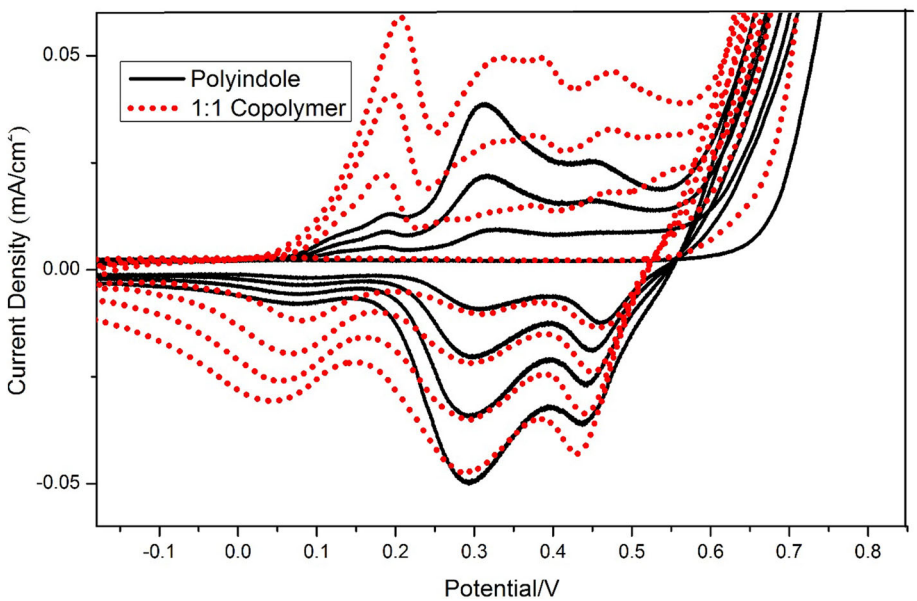

Fig. 8 Cyclic voltammogram of four continuous cycling for growing of 16 mM indole (black line) and **b** (1:1) indole-4aminoquinaldine (dot line) on ITO electrode in acetonitrile and 1 M $HClO_4$ (ACN:$HClO_4$ = 4:1 by vol.) mixture electrolyte. Potential scan rate: 80 mV/s

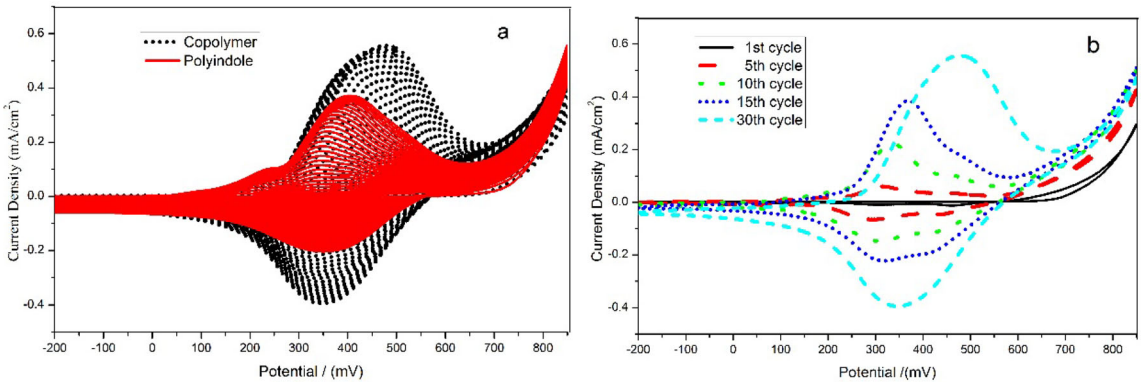

Fig. 9 Cyclic voltammogram of **a** Electropolymerization of indole and indole-4aq and **b** different cycle number (1st, 5th, 10th, 15th, and 30th) curves for growing 1:1 copolymer on ITO in acetonitrile and 1 M $HClO_4$ (ACN:$HClO_4$ = 4:1 by vol.) mixture electrolyte. Potential scan rate: 80 mV/s

to Faradaic's law [64]. This result implies that copolymer has a longer chain than that of polyindole. In Fig. 11b, the 1st, 5th, 10th, 15th, and 30th cycles of copolymer are shown. In Fig. 9b, the peak potentials shifting to a higher value may be due to the increased electrical resistance in the polymer film [65].

3.4.2 *Electrochemical characterization*

To determine the effects of each of the experimental variables (such as scan rate, scan number, and monomer concentration) on the electrochemical behavior of polymer films, polymer electrodes were immersed in 0.1 M $CuCl_2$ for 45 min. After, the immersed polymer film was washed with distilled water and was scanned in the 0.1 M KCl electrolyte from − 0.2 to 0.8 V at 20 mV/s.

First, the influence of monomer concentration on copolymer synthesis was investigated. For this purpose, indole concentration was fixed at 16 mM, and 4-aq concentrations were set at 8 mM, 16 mM, and 32 mM. Polymerization scan rate and cycle number were selected to be 80 mV/s and 30 cycle, respectively. From Fig. 10, it was observed that the copolymer 1:1 has a high anodic and cathodic current. It is seen from Fig. 10 that the voltammograms of polyindole and 0.5:1 copolymer include two waves in both the anodic and cathodic scans. However, when the concentration of 4-aq was increased, one wave was seen in both the anodic and cathodic scans. Further, it was observed that when the 4-aq concentration was dominant compared to the indole concentration in copolymer, the current decreased dramatically.

The concentration ratio of indole and 4-aq was fixed at 1:1, while other conditions of scan rate and scan number were determined. Copolymer was synthesized at different scan rates (50, 80, and 120 mV/s) and different scan numbers (10, 20, 30, and 40 cycles). Electroactivity of all copolymers was examined with the method mentioned above. As a result, other optimum conditions for synthesis of highly electroactive copolymer were found to be 80 mV/s and 30 cycles.

As mentioned previously, to identify and compare electroactivity of copolymer after each condition, all electrodes were immersed in a solution that includes Cu^{2+} ions. In order to determine the contribution of Cu^{2+} ions to the obtained result from cyclic voltammetry, the electrochemical measurements of the copolymer electrode were performed in three different experimental media.

1. CV was performed in 0.1 M KCl including 10 ml 0.1 M $CuCl_2$ (Fig. 11)
2. CV was performed in 0.1 M KCl media after the copolymer electrode was immersed for 45 min in 0.1 M $CuCl_2$ (Fig. 12-redline)
3. CV was performed in 0.1 M KCl without treatment of Cu^{2+} or adding Cu^{2+} (Fig. 12-blackline)

While the *I–V* curve in Fig. 11 shows the behavior of Cu^{2+}, the *I–V* curve in Fig. 12 shows the behavior of copolymer.

It can be seen from Fig. 12 that the current value of copolymer (red line) immersed in $CuCl_2$ is higher than copolymer (black line) that is not treated with Cu^{2+}. It can be concluded from these data that after

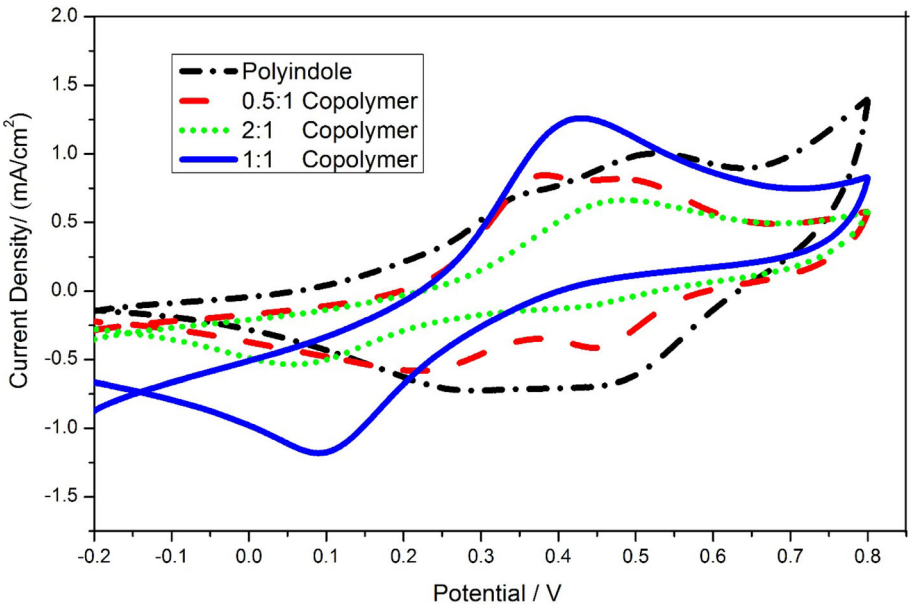

Fig. 10 Cyclic voltammogram of polyindole, 0.5:1, 1:1, and 2:1 copolymer in 0.1 M KCl at 20 mV/s

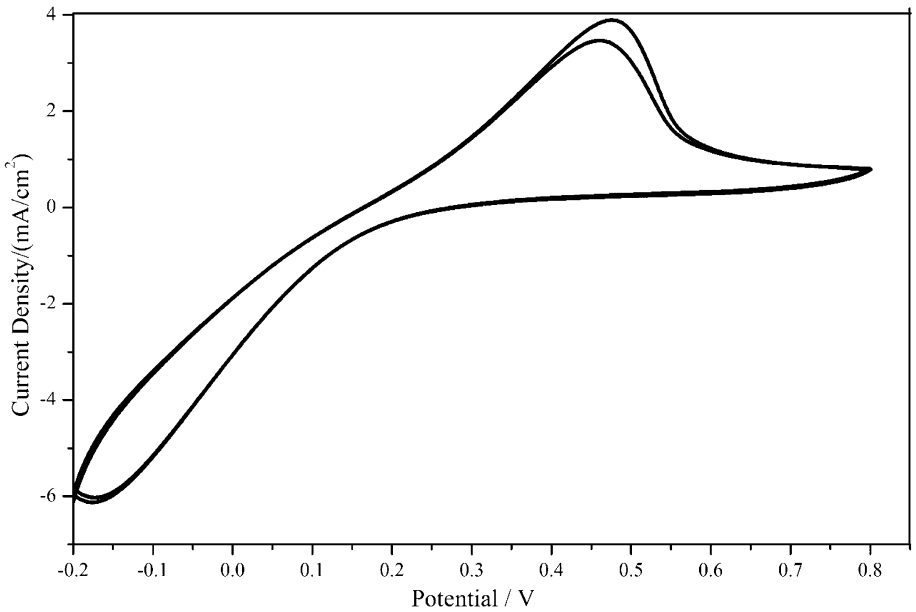

Fig. 11 Cyclic voltammogram of copolymer in 0.1 M KCl including 10 mL 0.1 M $CuCl_2$ at 20 mV/s

immersing the electrode in $CuCl_2$ solution, Cu^{2+} ions interact with copolymer physically which contributes to electron transfer and increased conductivity in the polymer. $CuCl_2$ is a stronger agent which promotes a high conductivity of polymer compared to other oxidizing agents such as $FeCl_3$, KIO_3 [66]. It was observed that the peak currents of the polymer film increased with the increasing adsorbed amount of Cu^{2+} ions on the polymer chain. To understand which electrode adsorbs more Cu^{2+} ions, a 1 ml sample was taken from the solution in which the electrode was immersed and analyzed by ICP-MS measurement. In the table, the values of the concentration of Cu^{2+} that is not adsorbed on polymer film are shown. As seen in Table 2, the adsorbed number of Cu^{2+} ions increased on the copolymer when compared to polyindole. This result may be related to the expanded active surface area of the copolymer.

In order to reveal whether Cu^{2+} ions are taking part in the copolymer chain, elemental mapping of the electrode was recorded. For this measurement, the electrode was kept in water for 1 h after being immersed in the $CuCl_2$ solution for 45 min. In Fig. 13, the elemental mapping shows that Cu^{2+} ions (signed

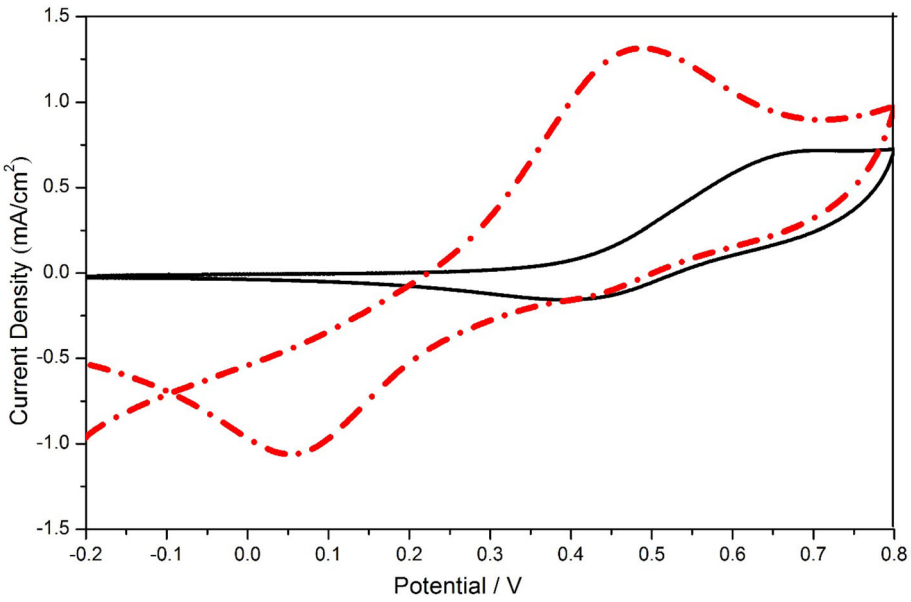

Fig. 12 Cyclic voltammogram of copolymer in 0.1 M KCl, (black line) non treatment, (dot line) after treatment with Cu^{2+} ions for 45 min

Table 2 Electrodes and the amounts of not adsorbed Cu^{2+} on their surface

Electrode	Concentration of Cu^{2+} (ppb)
Polyindole	6.028 × (250)[a]
0.5:1 copolymer	4.658 × (250)
1:1 copolymer	4.373 × (250)
2:1 copolymer	4.982 × (250)

[a]Dilution volume

with yellow point) are dispersed homogeneously on the copolymer (signed with red point).

3.4.3 *Electrochemical impedance spectroscopy*

The Nyquist and Bode plots of polyindole and copolymer in 0.5 M H_2SO_4 solution at − 0.6 V are shown in Figs. 14 and 15. The Nyquist diagrams show a depressed capacitive loop at high frequencies, followed by a linear tail at lower frequencies, which

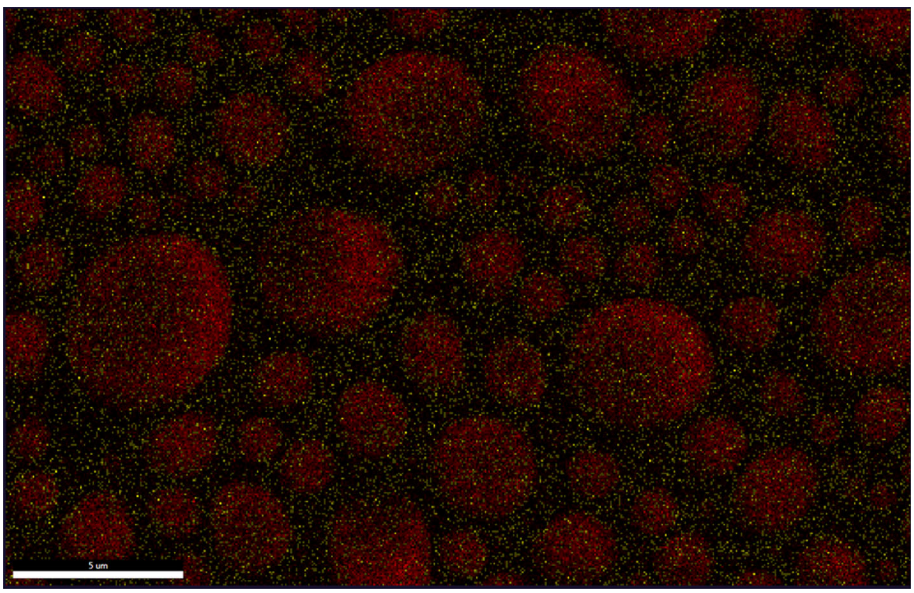

Fig. 13 Elemental mapping of Cu^{2+} ions that is adsorbed on copolymer

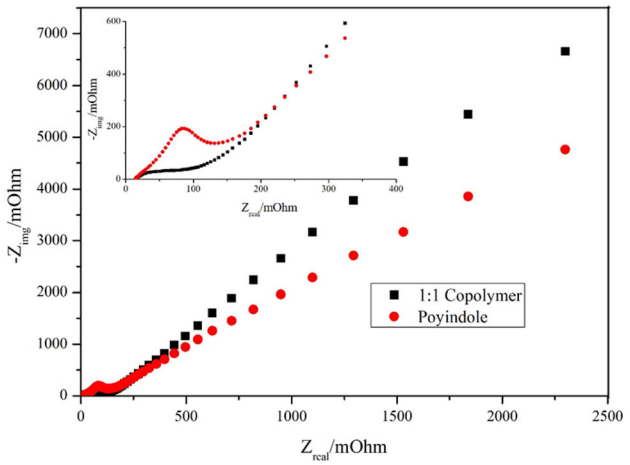

Fig. 14 The EIS spectrum recorded in 0.5 M H_2SO_4 for the 1:1 copolymer and polyindole. Inset shows the corresponding magnification of high frequency zone

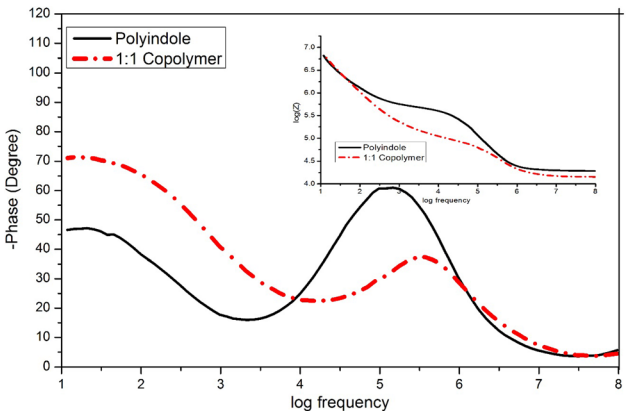

Fig. 15 Phase degree-log frequency and Bode (insert) plots of polyindole (black line), 1:1 Copolymer (dot line)

can be related to diffusion processes. The depressed semicircle observed at high frequencies is thought to correspond to the charge transfer resistance (R_{ct}) at the ITO/copolymer/electrolyte interfaces [67]. It was observed that the diameter of the capacitive loop at high frequency was decreasing for the copolymer.

The software (ZView2) was used to fit the EIS data. The fitting data show very good agreement with the corresponding experimental data (% error is shown in Table 3).The equivalent circuit (EC) proposed includes characteristic R_e, R_{CT}, and CPE components of the system (Fig. 16). R_e, R_{CT}, and CPE (constant phase element) represent the electrolytic resistance, the charge transfer resistance, and the electrode double layer capacitance, respectively. The CPE is used instead of the capacitance in order to account for the non-ideal behavior of the system. Also, the

Table 3 İmpedance fitting results for polyindole and copolymer on ITO

Electrode	Re (Ω)	CPE1-T (μF)	CPE1-P (n)	Rct (Ω)	W (Ω)
Polyindole	19.62	1.95e-5	0.94	423.4	5441
	(0.68)[a]	(3.7)	(0.56)	(1.48)	(5.79)
1:1 copolymer	14.37	3.59e-5	0.87	50.04	199.5
	(0.9)	(14.23)	(1.88)	(6.06)	(5.9)

[a](% error)

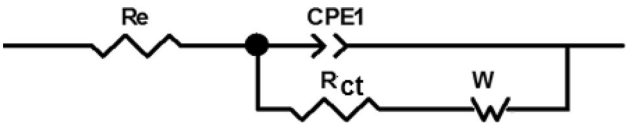

Fig. 16 Equivalent circuit used for simulation Nyquist diagram of polyindole and 1:1 copolymer

diffusion barrier that occurs in an electrochemical reaction causes the Warburg resistance, which is called the Warburg impedance (*W*) [67].

As can be seen from Table 3, the R_{ct} decreases dramatically and the CPE1 increases for the copolymer. It can be concluded that the possible reason for these observations is that the copolymer layers have high porosity. Additionally, Warburg resistance of the copolymer was reduced as a result of facilitating transport of the charge across the electrode/electrolyte interface. Besides, copolymer shows larger phase angle (− 72°) than polyindole (− 46°) corresponding to the high electrical conductivity and good ion diffusion capability in low frequency as can be seen in Fig. 15 [68].

4 Conclusions

In the present study, a novel copolymer, poly(indole-4aminoquinaldine), was synthesized both chemically and electrochemically. 4-aminoquinaldine was chosen as a second monomer that would increase both the conductivity and the N content of polyindole. The copolymer and polyindole were characterized by SEM–EDX, FTIR, UV, TGA, and XRD measurements and the data obtained were compared. Furthermore, the electrochemical activity of the copolymer was determined by alternative impedance spectroscopy and voltammetric methods. Additionally, monomer

concentration, scan rate, and scan number effect on copolymer structure were investigated.

According to the results of electrochemical measurements, to synthesize electroactive electrodes, optimum conditions are found to be 80 mV/s, 30 cycles, and 1:1 ratio of indole and 4-aminoquinaldine concentration. Furthermore, the 1:4 ratio of acetonitrile and 1 M $HClO_4$ is found to be the best media for deposition of copolymer. The synthesized highly electroactive novel copolymer that is named 1:1 copolymer has a porous structure, higher thermal stability, and conductivity than polyindole. The conductivity comparison of polyindole and copolymer was performed by four-point probe measurement, EIS, and the Tauc plot. According to these measurements, it was concluded that copolymer shows higher electron transfer mobility compared to polyindole. In brief, we demonstrated that polyindole properties improved by adding 4-aminoquinaldine as a second monomer for synthesis of copolymer. So, poly(indole-4aminoquinaldine) is a promising material in some potential applications such as electronic devices and sensors. In these applications, it can be used not only as a conductive supporting material but also as a N-precursor material to synthesize N-doped carbon-based electrodes.

Acknowledgements

The authors are thankful to the Mersin University research fund [2020-TP2-4009] for their financial support.

Author contributions

RSK: Writing—Original draft preparation, Experimental work. TA: Experimental work. MD: Reviewing and editing, Supervision.

Funding

Funding was provided by Mersin Üniversitesi (Grant No. 2020-TP2-4009).

Data availability

All data generated or analyzed during this study are included in this published article and its supplementary information files.

Declarations

Conflict of interest There are no conflicts of interest associated with this publication, and there has been no financial support for this work that could have influenced its outcome.

Research involving human and animal rights The authors emphasized that their study is not about human and animals.

Supplementary Information: The online version contains supplementary material available at https://doi.org/10.1007/s10854-022-08655-2.

References

1. S.J. Kwon, T.H. Han, T.Y. Ko, N. Li, Y. Kim, B. Kim, D.J. Yang, S.H.Y. Hong, Nat. Commun. (2018). https://doi.org/10.1038/s41467-018-04385-4
2. C.Y. Su, A.Y. Lu, Y. Xu, F.R. Chen, A.N. Khlobystov, L.J. Li, ACS Nano (2011). https://doi.org/10.1021/nn200025p
3. A. Ait, E. Fakir, Z. Anfar, M. Enneiymy, A. Jada, N. El, Appl. Catal. B (2022). https://doi.org/10.1016/j.apcatb.2021.120732
4. J. Wu, T. Sharifi, Y. Gao, T. Zhang, P.M. Ajayan, Adv. Mater. (2019). https://doi.org/10.1002/adma.201804257
5. H. Ning, Q. Mao, W. Wang, Z. Yang, X. Wang, Q. Zhao, Y. Song, M. Wu, J. Alloys Compd. (2019). https://doi.org/10.1016/j.jallcom.2019.01.142
6. U. Legrand, R. Boudreault, J.L. Meunier, Electrochim. Acta. (2019). https://doi.org/10.1016/j.electacta.2019.06.074
7. Y. Deng, Y. Xie, K. Zou, X. Ji, J. Mater. Chem. A (2015). https://doi.org/10.1039/c5ta08620e
8. X. Li, Y. Bai, M. Wang, G. Wang, Y. Ma, L. Li, B. Xiao, J. Zheng, Sustain Energy Fuels (2019). https://doi.org/10.1039/c9se00027e
9. S. Yuan, W. Chen, L. Zhang, Z. Liu, J. Liu, T. Liu, G. Li, Q. Wang, Small (2019). https://doi.org/10.1002/smll.201903311
10. J. Bao, J. Wang, Y. Zhou, Y. Hu, Z. Zhang, T. Li, Y. Xue, C. Guo, Y. Zhang, Catal. Sci. Technol. (2019). https://doi.org/10.1039/c9cy01182j
11. Z.J. Lu, S.J. Bao, Y.T. Gou, C.J. Cai, C.C. Ji, M.W. Xu, J. Song, R. Wang, RSC Adv. (2013). https://doi.org/10.1039/c3ra22161j

12. M. Ren, Z. Jia, Z. Tian, D. Lopez, J. Cai, M.M. Titirici, A.B. Jorge, ChemElectroChem (2018). https://doi.org/10.1002/celc.201800603
13. M. Du, J. Chang, F. Yang, L. Shi, L. Gao, RSC Adv. (2014). https://doi.org/10.1039/c4ra05544f
14. C.K. Maity, G. Hatui, K. Verma, G. Udayabhanu, D.D. Pathak, G.C. Nayak, Vacuum (2018). https://doi.org/10.1016/j.vacuum.2018.08.019
15. A.K. Mageed, R.A.B. Dayang, A. Salmiaton, S. Izhar, A. Razak, H.M. Yusoff, F.M. Yasin, S. Kamarudin (2016) http://www.ripublication.com.
16. D. Minta, Z. González, P. Wiench, S. Gryglewicz, G. Gryglewicz, Sensors (Switzerland). (2020). https://doi.org/10.3390/s20164427
17. J. Quílez-Bermejo, E. Morallón, D. Cazorla-Amorós, Polymers (Basel) (2020). https://doi.org/10.3390/polym12102382
18. G. Qi, L. Huang, Wang, Chem. Commun. **48**, 8246–8248 (2012). https://doi.org/10.1039/C2CC33889K
19. T. Zhu, J. Zhou, Z. Li, S. Li, W. Si, S. Zhuo, J. Mater. Chem. A (2014). https://doi.org/10.1039/c4ta01465k
20. A.A. Ramachandran, J.S. Nair, Y.S. Karunakaran, ACS Sustain. Chem. Eng. (2019). https://doi.org/10.1021/acssuschemeng.8b05996
21. K. Cong, M. Radtke, S. Stumpf, B. Schröter, D.G.G. McMillan, M. Rettenmayr, A. Ignaszak, Mater. Renew. Sustain. Energy (2015). https://doi.org/10.1007/s40243-015-0046-9
22. M. Sevilla, P. Valle-Vigõn, A.B. Fuertes, Adv. Funct. Mater. (2011). https://doi.org/10.1002/adfm.201100291
23. A. Ait El Fakir, Z. Anfar, A. Amedlous, M. Zbair, Z. Hafidi, M. El Achouri, A. Jada, N. El Alem, Appl. Catal. B (2021). https://doi.org/10.1016/j.apcatb.2021.119948
24. J. Wu, W. Zhou, F. Jiang, Y. Chang, Q. Zhou, D. Li, G. Ye, C. Li, G. Nie, J. Xu, T. Li, Y. Du, A.C.S. Appl, Energy Mater. (2018). https://doi.org/10.1021/acsaem.8b00722
25. I. Marriam, Y. Wang, M. Tebyetekerwa, Energy Storage Mater. (2020). https://doi.org/10.1016/j.ensm.2020.08.010
26. A.P. Syed, R. Saraswathi, Org. Electron. (2004). https://doi.org/10.1016/j.orgel.2004.10.002
27. S.A. Yerişkin, H.I. Unal, B. Sarı, J. Appl. Polym. Sci. (2011). https://doi.org/10.1002/app.33148
28. S. Podder, S. Paul, P. Basak, B. Xie, N.J. Fullwood, S.J. Baldock, Y. Yang, J.G. Hardy, C.K. Ghosh, RSC Adv. (2020). https://doi.org/10.1039/d0ra01129k
29. N.K. Guimard, N. Gomez, C.E. Schmidt, Prog. Polym. Sci. (2007). https://doi.org/10.1016/j.progpolymsci.2007.05.012
30. A. Lendlein, M. Rehahn, M.R. Buchmeiser, R. Haag, Macromol. Rapid Commun. (2010). https://doi.org/10.1002/marc.201000426
31. İ Gergin, A.T. Gökçeören, A.S. Sarac, Fibers Polym. (2015). https://doi.org/10.1007/s12221-015-5144-x
32. K. Phasuksom, W. Prissanaroon-Ouajai, A. Sirivat, Sensors Actuators B (2018). https://doi.org/10.1016/j.snb.2018.02.088
33. M. Düdükcü, F. Köleli, Prog Org Coatings (2006). https://doi.org/10.1016/j.porgcoat.2006.01.004
34. T. Tüken, B. Yazici, M. Erbil, Surf. Coatings Technol. (2006). https://doi.org/10.1016/j.surfcoat.2005.04.023
35. T. Tüken, M. Düdükçü, B. Yazici, M. Erbil, Prog Org. Coatings. (2004). https://doi.org/10.1016/j.porgcoat.2004.03.004
36. A. Verma, R.B. Choudhary, Mater. Sci. Semicond. Process. (2020). https://doi.org/10.1016/j.mssp.2020.104948
37. E. Dogan, E. Ozkazanc, H. Ozkazanc, Synth. Met. (2019). https://doi.org/10.1016/j.synthmet.2019.116154
38. Y. Wang, T. Wang, T. Wang, J. Zhang, J. Chen, R. Yang, L. Ruan, B. Wang, Polym. Eng. Sci. (2019). https://doi.org/10.1002/pen.24839
39. Y. Wang, H. Yu, Y. Li, T. Wang, T. Xu, J. Chen, Z. Fan, Y. Wang, B. Wang, Polymers (Basel) (2019). https://doi.org/10.3390/polym11030546
40. G. Qi, L. Huang, H. Wang, Chem. Commun. (2012). https://doi.org/10.1039/c2cc33889k
41. K. Phasuksom, A. Sirivat, Synth. Met. (2016). https://doi.org/10.1016/j.synthmet.2016.05.033
42. V. Arjunan, I. Saravanan, P. Ravindran, S. Mohan, Spectrochim. Acta Part A (2009). https://doi.org/10.1016/j.saa.2009.06.028
43. V. Krishnakumar, R.J. Xavier, Chem. Phys. (2005). https://doi.org/10.1016/j.chemphys.2004.11.016
44. D. Caldwell, W.A. Cox, P.F. D'Arcy, L.R. Rowe, J. Pharm. Pharmacol. (1961). https://doi.org/10.1111/j.2042-7158.1961.tb11869.x
45. M. Düdükcü, G. Avcı, Res. Chem. Intermed. (2015). https://doi.org/10.1007/s11164-014-1572-2
46. M.A. El-Attar, I.M. Ismail, M.M.J. Ghoneim, Braz. Chem. Soc. (2012). https://doi.org/10.1590/S0103-50532012005000013
47. A.A. Hathoot, M. Abdel-Kader, M. Abdel-Azzem, Int J Electrochem. Sci. **4**, 208–222 (2009)
48. M.A. Azzem, Eur. Polym. J. (1993). https://doi.org/10.1016/0014-3057(94)00123-5
49. L. Xu, D. Li, W. Zhou, Y. Ding, Y. Wu, J. Xu, X. Duan, Arab. J. Chem. (2020). https://doi.org/10.1016/j.arabjc.2020.05.006
50. S. Mozaffari, J. Behdani, S.M.B. Ghorashi, Polym. Bull. (2021). https://doi.org/10.1007/s00289-021-03833-4
51. G. Shanmugam, S. Brahadeeswaran, Spectrochim. Acta Part A (2012). https://doi.org/10.1016/j.saa.2012.04.100

52. H.K. Rasheed, A.A. Kareem, J. Opt. Commun. (2021). https://doi.org/10.1515/joc-2018-0024
53. C.J. Verma, R.K. Pandey, R. Prakash, Mater. Sci. Eng. B (2018). https://doi.org/10.1016/j.mseb.2017.10.015
54. L. Joshi, A.K. Singh, R. Prakash, Mater. Chem. Phys. (2012). https://doi.org/10.1016/j.matchemphys.2012.04.026
55. R.X. Wang, Y.J. Fan, L. Wang, L.N. Wu, S.N. Sun, S.G. Sun, J. Power Sources (2015). https://doi.org/10.1016/j.jpowsour.2015.03.181
56. N. Puviarasan, V. Arjunan, S. Mohan, Turk. J. Chem. **28**(1), 53–66 (2004)
57. J. Arjomandi, H. Soleimani, M.H. Parvin, E. Azizi, Polym. Compos. (2019). https://doi.org/10.1002/pc.24674
58. P. Chattıse, K. Handore, A. Horne, K. Mohıte, A. Chaskar, S. Dallavalle, V. Chabukswar, J. Chem. Sci. (2016). https://doi.org/10.1007/s12039-016-1040-1
59. A. Şelte, B. Özkal, Proc. Est. Acad. Sci. (2019). https://doi.org/10.3176/proc.2019.1.02
60. M. Warczak, M. Osial, M. Berggren, E.D. Glowacki, J. Electrochem. Soc. (2020). https://doi.org/10.1149/1945-7111/ab88bb
61. R. Yue, F. Jiang, Y. Du, J. Xu, P. Yang, Electrochim. Acta. (2012). https://doi.org/10.1016/j.electacta.2012.05.150
62. B. Gupta, A.K. Singh, A.A. Melvin, R. Prakash, Solid State Sci. (2014). https://doi.org/10.1016/j.solidstatesciences.2014.05.015
63. M.B. Camarada, P. Jaque, F.R. Díaz, M.A. Del-Valle, J. Polym. Sci. Part B (2011). https://doi.org/10.1002/polb.22360
64. A.N. Grace, S.Y. Choi, M. Vinoba, M. Bhagiyalakshmi, D.H. Chu, Y. Yoon, S.C. Nam, S.K. Jeong, Appl. Energy. (2014). https://doi.org/10.1016/j.apenergy.2014.01.022
65. H.-M. Miao, H.-L. Zhang, J.-K. Xu, C.-L. Fan, B. Dong, L.-Q. Zeng, F. Zhao, Chin. J. Chem. (2008). https://doi.org/10.1002/app.21532
66. D. Billaud, E.B. Maarouf, E. Hannecart, Chemical oxidation and polymerization of indole. Synth. Met. **69**, 571–572 (1995). https://doi.org/10.1016/0379-6779(94)02573-H
67. K.R.L. Castagno, V. Dalmoro, D.S. Azambuja, Mater. Chem. Phys. (2011). https://doi.org/10.1016/j.matchemphys.2011.07.052
68. T. Li, Y. Zhou, Z. Dou, L. Ding, S. Dong, N. Liu, Z. Qin, Electrochim. Acta. (2017). https://doi.org/10.1016/j.electacta.2017.05.087